Brazilian Journal of Analytical Chemistry
Pre-publication – Accepted after peer review
doi: 10.30744/brjac.2179-3425.AR-70-2025

BrJAC

ARTICLE

Evaluation of *Calendula officinalis* Extract as a Functionalization Agent for Gold Nanoparticles

Comprehensive Multi-Technique Analytical Characterization and its use as a Dye-Sensitized Solar Cell Sensitizer

Mauricio Ávila[1]*, Hiroyuki Kinoshita[1], Pablo Fagúndez[2], María Fernanda Cerdá[1]

[1]*Laboratorio de Biomateriales, Instituto de Química Biológica, Facultad de Ciencias, Universidad de la República. Iguá 4225, Anexo Norte, Piso 2, Laboratorio 205, Zip Code 11400, Montevideo, Uruguay*

[2]*Unidad de Bioquímica Analítica, Centro de Investigaciones Nucleares, Universidad de la República. Mataojo 2055, Zip Code 11400, Montevideo, Uruguay*

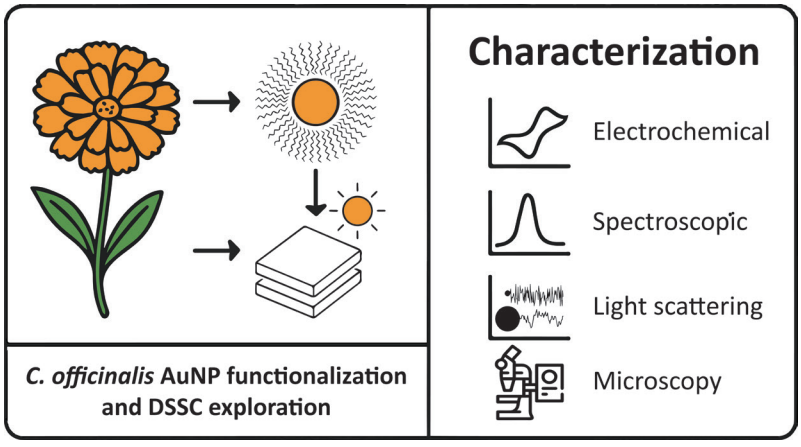

Calendula officinalis extract was evaluated as a functionalization agent for gold nanoparticles (AuNPs). The resulting nanoconjugate (AuNP-Cale) was thoroughly characterized, and explored as a sensitizer for dye-sensitized solar cells (DSSC). As a starting point, citrate-reduced AuNPs (AuNP-Cit) were synthesized and fully characterized. Comprehensive characterization for both AuNP-Cit and AuNP-Cale included dynamic light scattering (DLS), electrophoretic light scattering (ELS), colloidal and stability assay. Successful functionalization included increased hydrodynamic diameter, reduced zeta potential, and improved colloidal stability. DSSC evaluation demonstrated that while pre-formed AuNP-Cale did not enhance efficiency, improved performance was achieved when AuNP-Cit was added sequentially after the extract on the TiO_2 electrode, likely due to better electrode coverage. This result correlated with enhanced light absorption (FORS) and favorable electrochemical impedance spectroscopy parameters.

Keywords: gold nanoparticles, functionalization, spectroscopy, voltammetry, dye-sensitized solar cells

Cite: Ávila, M.; Kinoshita, H.; Fagúndez, P.; Cerdá, M. F. Evaluation of *Calendula officinalis* Extract as a Functionalization Agent for Gold Nanoparticles – *Comprehensive Multi-Technique Analytical Characterization and its use as a Dye-Sensitized Solar Cell Sensitizer*. *Braz. J. Anal. Chem.* (Forthcoming). http://dx.doi.org/10.30744/brjac.2179-3425.AR-70-2025

Submitted: July 29, 2025; **Revised:** September 22, 2025; November 3, 2025; **Accepted:** November 30, 2025; **Published online:** January 2026.

This article was submitted to the BrJAC special issue on the 8th Uruguayan Congress of Analytical Chemistry (CUQA 8 2024).

INTRODUCTION

The XXI century is the time for nanotechnologies. The term “nanotechnology” was first used by the eminency of Richard P. Feynman in 1960.[1] Nanotechnology is the scientific discipline that studies, designs and applies materials, devices and systems at the nanometric scale, including particulate substances, which have at least one dimension less than 100 nm.[2] In the continued search for better and smaller devices, properties related to the use and applications of nanoparticles became relevant. Examples of nanoparticle applications are everywhere, comprising pharmaceutical,[3-5] properties modification for manufacturing materials,[6-8] environment,[9-10] electronics,[11-14] energy,[15-20] and informatics[21-23] just to name a few.

Gold nanoparticles (AuNPs) exhibit unique optical properties among the metallic nanoparticles due to localized surface plasmon resonance (LSPR), which can enhance light absorption and energy transfer in dye-sensitized solar cells (DSSC).[20,24-29]

Metallic nanoparticles, particularly AuNPs, have experienced a significant boom in scientific research since the 1990s, although their use dates back to ancient times in the coloration of glasses and ceramics.[30] Interest in AuNPs has intensified due to advances in characterization and synthesis techniques and their consequent improvement in the ability to control size, shape and surface properties.[31] In addition, the diverse applications of AuNPs are due to their exceptional optical, electronic and catalytic properties.[32]

In the field of energy and optoelectronics, they stand out for their ability to improve solar cell efficiency through the plasmonic effect,[33] which allows for increased light absorption and energy transfer. Their unique properties derive mainly from localized surface plasmon resonance (LSPR), a phenomenon resulting from the collective oscillation of free electrons at the nanoparticle surface in response to incident electromagnetic radiation.[34,35] This feature gives AuNPs their distinctive colors and makes them especially valuable in applications requiring efficient interaction with light, such as optical sensors and photovoltaic devices.[36]

Functionalizing AuNPs with different ligands can modify their surface properties, stability and interactions with other molecules in the system under evaluation.[37] In this context, the present study explores using *Calendula officinalis* extract for AuNPs derivatization.

Calendula officinalis is an annual perennial flowering plant in the family Asteraceae, native to southern Europe and cultivated worldwide for medicinal, ornamental, and culinary purposes.[38] This plant has vibrant orange-yellow daisy-like flowers with multiple layers of overlapping petals and aromatic leaves.[39] *Calendula officinalis* extracts have around 7.71% (w/w) carotenoids (mainly flavoxanthin, luteoxanthin, and lycopene, Figure 1),[39] 0.21-0.68% (w/w) of flavonoids (mainly rutin, isorhamnetin and isoquercitrin),[39-42] and xanthophylls.[43] Many of these compounds have functional groups as hydroxyl moieties, making them an attractive option for nanoparticle functionalization.

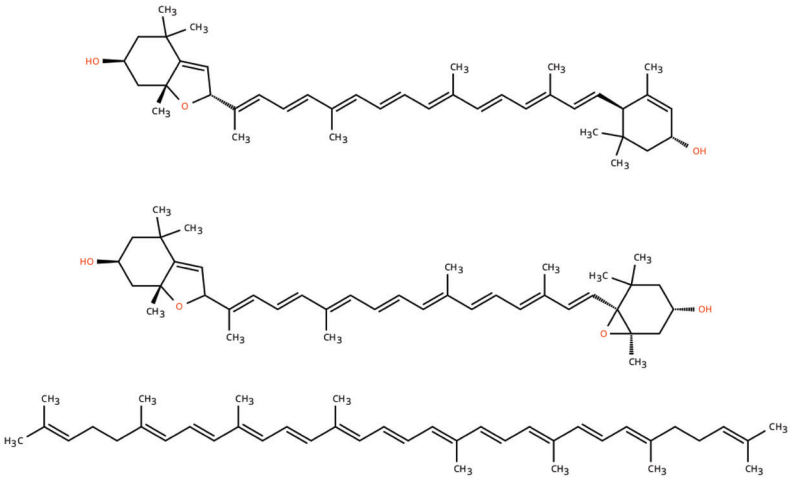

Figure 1. The three main carotenoids present in *Calendula officinalis.* From top to bottom: flavoxanthin, luteoxanthin and lycopene.

Normally, the synthesis of biogenic AuNPs is performed using the natural extract as both a reducing and capping agent. However, it is often difficult to control the shape and size of the obtained nanoparticles, since the concentration and type of reducing agent are not known with certainty, and the amount of this agent can vary from one extract to another.[44-46] In this regard, we approached the initial synthesis of AuNPs using classical, more controlled methods, which allow precise control of the Au/reducing agent molar ratio, and then proceeded with post-synthesis functionalization using calendula extract following the standard adsorption procedure described in the literature. No previous reports were found on post-synthesis functionalization of AuNPs with calendula's extract. However, there are reports of direct synthesis of gold, silver, and titanium nanoparticles from calendula extract, where stable nanoparticles are obtained, confirming the extract's ability not only to provide a reducing agent but also to contribute stabilizing molecules to the colloidal system.[47-50]

In this work we derivatize AuNPs with *Calendula officinalis* extract and exhaustively characterize the nanoconjugate AuNP-Cale. The research encompasses synthesizing and characterizing functionalized AuNPs, including comprehensive analysis through UV-Vis spectrophotometry, dynamic light scattering (DLS), electrophoretic light scattering (ELS), colloidal stability assay, transmission electron microscopy (TEM), and cyclic voltammetry studies.

To essay on a possible technological application, dye-sensitized solar cells (DSSC) performance is evaluated by incorporating AuNPs functionalized with *Calendula officinalis* extract, since the use of metal nanoparticles has been reported to increase the performance of dye-sensitized solar cells.[51] In this case, the performance of the DSSC was evaluated by measuring the current-voltage (J-V) profiles under both illumination and dark conditions, complemented by electrochemical impedance spectroscopy (EIS). To understand the performance of the assembled DSSC, spectroscopic characterization of the sensitizers was performed using reflectance spectrophotometry and Fourier transform infrared (FTIR) analyses (before and after adsorption to the semiconductor of the photoanode). This comparative study involves cells with functionalized AuNP-Cale, AuNP-Cit, and calendula's extract without nanoparticles, providing an insight into the capability of *Calendula officinalis* extract as a dye for DSSC purposes.

MATERIALS AND METHODS

Materials and chemicals

Chloroauric acid ($HAuCl_4.3H_2O$ ≥ 99.9%, CAS No. 16961-25-4), trisodium citrate dihydrate ($Na_3C_6H_5O_7.2H_2O$ ≥ 98%, CAS No. 6132-04-3), sodium chloride (NaCl ≥ 99%, CAS No. 7647-14-5), and sodium perchlorate ($NaClO_4$ ≥ 98%, CAS No. 7601-89-0), were purchased from Sigma-Aldrich. Potassium bromide (KBr, FTIR grade, CAS No. 7758-02-3) was purchased from Pike Technologies. Absolute ethanol (≥ 99.8%, CAS No. 64-17-5) and heptane (≥ 99%, CAS No. 142-82-5) were obtained from Dorwil, Química Analítica. Ultrapure water (resistivity > 18.2 MΩ·cm, Millipore Milli-Q®) was used throughout. DSSC components (FTO/TiO_2 electrodes, Pt counter electrodes, Iodolyte AN-50 electrolyte) were purchased from Solaronix. All chemicals were used as received without further purification.

Calendula officinalis dyes extraction

The *Calendula officinalis* flowers were collected from the "Universidad de la República, Facultad de Ciencias", orchard at the beginning of October 2024 (southern hemisphere's spring).

Petals from 20 flowers were collected, chopped, and mortared with absolute ethanol. Samples were ultrasounded for 15 minutes, vortexed, and centrifuged for 15 minutes at 5000 rpm, preserving the supernatant. After extracting the supernatant, the same procedure was done from the pellet. Two extractions were obtained; the first (denoted 1E) was the extraction without resuspension, and the second (denoted 2E) was the extraction plus the resuspension.

Samples were withdrawn, and heptane-ethanol phase separation was performed to eliminate chlorophyll. The remaining ethanolic phase did not significantly differ from the fraction before the phase separation, so for practical purposes, extraction 2E without heptane purification was used.

AuNP-Cit synthesis

The glassware used in the synthesis and storage of AuNPs was previously treated with an aqua regia solution ($HCl:HNO_3$ 3:1 (v/v)) for 30 min, subsequently rinsed with abundant ultrapure water (resistivity > 18.2 MΩ.cm) and dried in an oven at 60 °C prior to use. The synthesis of AuNPs was carried out according to the traditional Turkevich method with modifications. Briefly, 50 mL of ultrapure water and 1 mL of a 20 g L^{-1} chloroauric acid solution (≈ 50 µmol) were placed in a two-neck round-bottom flask, and the system was completed with a water condenser. The solution was heated to boiling and 5 mL of 38.8 mM sodium citrate solution was immediately added. The solution was continued to be heated under reflux until the appearance of an intense red-burgundy color and maintained for an additional 10 min. The AuNP-cit solution was allowed to cool for 24 h in the dark before characterization.[52-55]

AuNP-Calendula officinalis extract derivatization

For derivatization, the citrate-reduced gold nanoparticles (AuNP-Cit) were obtained by the Turkevich method.[56] After that, the AuNP-Cit were incubated overnight in the presence of the *Calendula officinalis* extract using a 9:1 (v:v) AuNP-Cit:Cale proportion.

UV-Vis absorption spectrophotometry

The UV-Vis spectra were acquired with an Analytic-Jena SPECORD 200 Plus spectrophotometer only in the range from 350 to 700 nm, using the optical path b = 1 cm. Spectrometer increments were set at 0.05 nm.

Dynamic light scattering

Dynamic light scattering was performed to determine the average hydrodynamic diameter (d_h) of both AuNP-Cit and AuNP-Cale using the Brookhaven ZetaPlus 90 instrument equipped with a 659 nm laser and a correlator. DLS measurements were conducted at a fixed angle of 90 degrees in 1 cm polystyrene cuvettes following ISO 22412 guidelines.[57]

Transmission electron microscopy

AuNP-Cit's diluted colloidal solutions (10 µL, 1:10 in water) were drop-casted to a carbon-coated copper grid and air-dried at room temperature. TEM images were captured using a JEOL JEM 1010 microscope at an acceleration voltage of 80 kV. The diameters (d_{TEM}) of over 200 individual AuNPs were determined from 10 micrographs using FIJI software,[58] following the previously established guidelines.[59,60]

Electrophoretic light scattering

Electrophoretic light scattering was performed to determine the zeta potential (ζ-potential) of the AuNPs with the same equipment and configuration as DLS. Additionally, a fixed angle of 15° was used with a surface zeta potential (SZP) electrode system consisting of two parallel palladium electrodes. All measurements were performed at 25 °C using a 1 nM AuNP solution in 1 mM NaCl. The data (n = 6) was analyzed using Particle Solution v. 2.5 software, applying CONTIN and Smoluchowski algorithms for hydrodynamic diameter and ζ-potential calculations, respectively.

Colloidal stability assay

Colloidal stability was determined using a simplified, rapid screening version of the colloidal stability titration assay with a Tekan Infinite F50 microplate reader adapted from the methodology described in the literature[61] and detailed in our previous work.[56]

In a 96-well microplate, 100 µL of the AuNP-Cit or AuNP-Cale was added. To each well, 100 µL of a 20 to 300 mM sodium chloride (NaCl) solution (NaCl final concentration 10 to 150 mM) was added. After mixing, absorbance was measured at 520 nm and 650 nm.[56] All measurements were duplicated. The Boltzmann sigmoidal equation's inflexion point on the curve determined the critical concentration. Boltzmann sigmoidal fitting was performed using the Levenberg-Marquart iteration algorithm.

Infrared spectroscopy

Infrared spectra were collected in the 400-3000 cm^{-1} range at ambient temperature using a Shimadzu IR-Prestige 21 spectrometer. Each spectrum represented an average of 10 scans with 2 cm^{-1} resolution. Sample preparation involved thoroughly mixing dried samples with KBr powder in an agate mortar, followed by forming 13-mm discs using a Pike Crush IR press at 10 tons of pressure. For comparative purposes, the following samples were analyzed: Cale, AuNP-Cit, AuNP-Cale, and these three samples after being deposited onto TiO_2 electrodes (TiO_2:Cale, TiO_2:AuNP-Cit, and TiO_2:AuNP-Cale). For the TiO_2-deposited samples, the same procedure was followed as previously described, where the electrode surface was scraped off after the adsorption period, mixed with KBr, and pressed into discs.

Cyclic voltammetry

All reagents were used as received from commercial sources without further purification. The voltammetric profiles were conducted using a Metrohm μStat-i 400 s Potentiostat in a one-compartment conic cell three-electrode system. Since EtOH was the extraction media, samples were measured in mixtures EtOH:supporting electrolyte (0.1 M sodium perchlorate $NaClO_4$ in high-purity MilliQ® water 18.2 MΩ.cm) in a proportion 1:1 (v:v). Evaluations were then performed using 1 mM of the analyte in the described mixture of solvents. The working electrode (W) was FTO/TiO_2 (FTO = Fluorine-doped Tin Oxide; TiO_2 = mesoporous titanium dioxide), and the auxiliary electrode (A) was made of Pt-*pc* (*pc* = polycrystalline). The reference electrode (R) was the silver/silver chloride (Ag/AgCl; E = 0.2586 V *vs.* NHE). All measurements were performed at a scan rate of 50 mV s^{-1}.

Dye sensitized solar-cell built-up and evaluation

Photoanodes were prepared by immersion of the FTO/TiO_2 (SOLARONIX test kit, active area of mesoporous TiO_2 0.36 cm^2) electrodes overnight into the dye's containing solution and then rinsed thoroughly with ethanol. Before use, the FTO/TiO_2 electrode was heated at 500 ºC for 30 minutes. A sandwich configuration was used, with the FTO/TiO_2 photoanode placed parallel to the FTO/Pt counter (20 mm x 20 mm sized, screen printed with SOLARONIX's Pt Platinum Catalyst). The cell was then completed by the addition of a liquid electrolyte (SOLARONIX Iodolyte AN-50). Different sensitizers were applied: Cale, AuNP-Cit, AuNP-Cale and Cale co-sensitized with AuNP following a sequential path.

To characterize the DSSC, the current density *vs.* voltage (J-V) profiles were measured using a CHI 604E potentiostat at a potential scan rate (*v*) of 0.05 V s^{-1} at room temperature, in the dark and using a solar simulator from ABET Technologies (100 mW cm^{-2}, 1.5 AM). Complementary data were assessed from the electrochemical impedance spectroscopy (EIS) results, performed between 0 and 0.5 V and within the frequency range of 0.1 Hz to 3 MHz (in the dark).

Fiber optic reflectance spectroscopy

Fiber optic reflectance spectroscopy (FORS) was employed to verify the incorporation of AuNP-Cale, AuNP-Cit and Cale within the TiO_2 matrix. Average reflectance measurements of 500 spectra were conducted using a UV-Vis SPELEC (200-900 nm) instrument (DROPSENS) equipped with a fiber optic probe. FTO/TiO_2 electrodes were immersed overnight with the corresponding solution. Prior to spectroscopic analysis in the 350–850 nm wavelength range, the electrodes were thoroughly rinsed with ethanol to remove any unbound components. This technique allowed for non-destructive confirmation of the adsorption onto the TiO_2 surface.

RESULTS AND DISCUSSION

Synthesis and characterization of functionalized gold nanoparticles

Calendula officinalis dyes extraction

After the extraction of *C. officinalis*, UV-Vis spectra were performed, and serial dilutions were performed until the absorbances measured were above 1 UA to calculate carotenoid concentration in the extract, according to the extinction coefficient estimation by Britton et al. 2004 (Figure 2).[62]

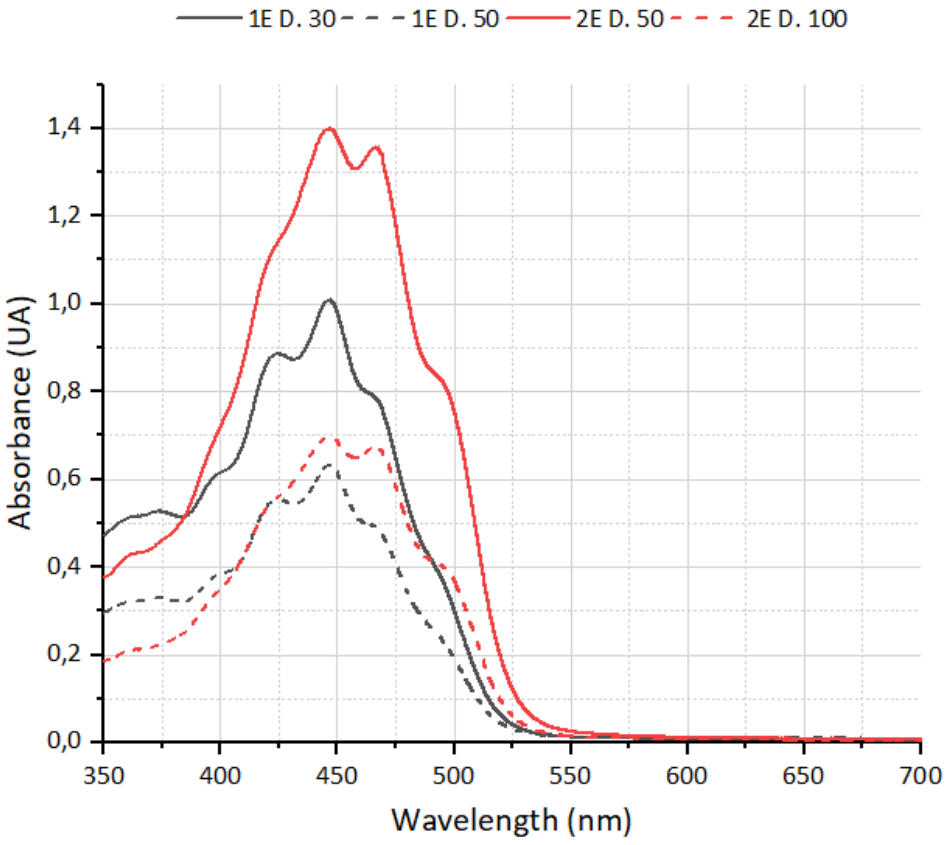

Figure 2. UV-Vis spectra of solutions containing the extracts from *Calendula officinalis*. Black lines correspond to the first extraction (in legend denoted 1E), while red lines correspond to the second extraction (in legend denoted 2E). The dilution factor for each spectrum is shown in the legend above. Being the most diluted fraction drawn in dashed lines.

Based on the extinction coefficients calculated following Britton et al. (2004)[62] and absorbance measurements at the characteristic carotenoid maximum (447 nm), the total carotenoid concentrations were determined to be 0.196 ± 0.006 mM for the first extraction (1E) and 0.442 ± 0.002 mM for the second extraction (2E). Due to its higher concentration and comparable spectral profile, extraction 2E was selected for all subsequent functionalization experiments (see calculations in the Supplementary Material).

Citrate-reduced gold nanoparticles characterization

Prior to functionalization with *Calendula officinalis* extract, the citrate-stabilized gold nanoparticles (AuNP-Cit) were thoroughly characterized. UV-Vis spectroscopy revealed a characteristic localized surface plasmon resonance (LSPR) peak at 520 nm (Figure SM-1). Transmission electron microscopy (TEM) analysis demonstrated that the synthesized AuNP-Cit exhibited a predominantly spherical morphology with an average diameter of d_{TEM} = (16 ± 3) nm (Figure 7). Dynamic light scattering (DLS) measurements indicated a hydrodynamic diameter of d_h = (19 ± 3) nm with a polydispersity index (PDI) of 0.23 ± 0.03 (Figure SM-2). The zeta potential value of (-52 ± 2) mV confirmed the presence of negatively charged citrate ions on the nanoparticle surface, providing electrostatic stabilization and preventing aggregation in aqueous solution. These baseline characteristics of AuNP-Cit serve as a reference point for evaluating the subsequent modifications introduced by *Calendula officinalis* extract functionalization. Similar results were obtained by Méndez et al.[55] and Fagúndez et al.[56]

AuNP-Cit:EtOH ratio optimization

As stated, *Calendula officinalis* dyes were extracted using ethanol. Since EtOH is less polar than water, it alters the colloidal stability of AuNP-Cit by shielding the charge between citrate molecules. Also, the presence of EtOH reduces the dielectric constant in the media, which, in turn, lowers the repulsion between AuNP-Cit. In sum, these effects tend to aggregate AuNP-Cit particles, so prior to the AuNP-Cale derivatization, the AuNP-Cit aqueous solution to EtOH relation was optimized by diluting AuNP-Cit in EtOH, and UV-Vis spectra were recorded (Figure SM-3).

It is clear from Figure SM-3 that AuNPs aggregate when the proportion of AuNP-Cit to EtOH is greater than 1:4. This is concluded based on the position of the localized surface plasmon resonance (LSPR), which has its maxima near 520 nm when AuNPs are not aggregated, and bathochromic shifts due to plasmonic coupling towards 620 nm when AuNPs aggregate. That is, higher AuNP-Cit to EtOH proportions diminish its absorbance at 520 nm and increase the absorbance at 620 nm, suggesting a shift of AuNPs from a non-aggregated to an aggregated state. In the case of 1:4 proportion, this mixture was borderline aggregation, so for conservative reasons 1:9 was the proportion against EtOH chosen for further analysis.

UV-Vis absorption spectrophotometry and LSPR position

Once the optimal AuNP-Cit with *Calendula officinalis* extract relation was determined, a fast procedure for AuNP-Cit derivatization with calendula extract confirmation was established as follows: Firstly, AuNP-Cit UV-Vis spectra were taken in serial dilutions. The LSPR position was determined by taking the point where the derivative of $d_{Abs}/d\lambda = 0$ (λ_{LSPR} = 519 nm) and at the mentioned wavelength absorbance was measured for every dilution, generating the calibration curve in Figure 3.

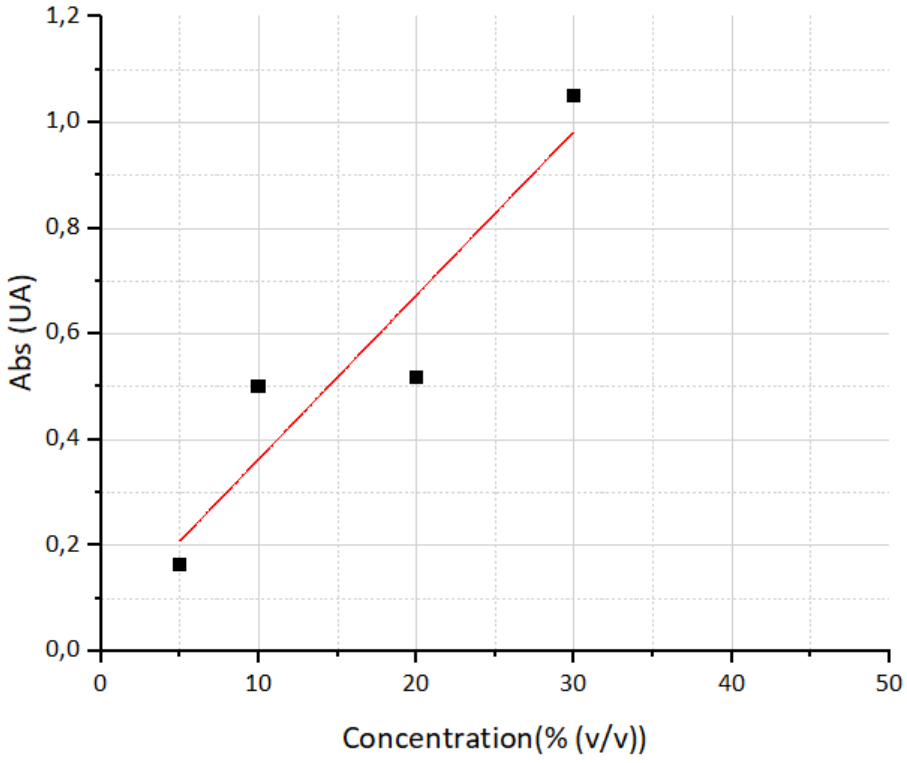

Figure 3. The absorbance at the LSPR wavelength (λ = 519 nm) was plotted as a function of AuNP-Cit concentration (% v/v), where 100% is the Turkevich synthesis product ([AuNP] ≈ 10 nM). The linear relationship y = (0.036 ± 0.002)x – (0.03 ± 0.03), R^2 = 0.993, followed by ANOVA analysis demonstrates that absorbance is an additive property within the measured range (0 – 30% v/v), following the Beer-Lambert law.

Lastly, the same procedure was followed with AuNP-Cale (calendula extract to AuNP-Cit 1:9 v/v proportion) and water dilutions as shown in Figure SM-4. From the mentioned figure, UV-Vis spectra were taken, derivatives were calculated, and the point where $d_{Abs}/d\lambda = 0$ was measured only for the peak corresponding to AuNP LSPR signal. By so doing, the LSPR position turned out to be λ_{LSPR} = 510 nm, showing a clear hypsochromic shift from the AuNP-Cit. Usually, the λ_{LSPR} shifts towards a greater wavelength since it is proportional to the media dielectric (ε). So, functionalizing with greater molecules augments ε concomitant to λ_{LSPR} bathochromic shifts. On the contrary, a hypsochromic shift was observed. Two hypotheses are proposed: (*i*) the extract's carotenoids could interact with the conjugated π electrons, which could be "extracting" electronic density from the plasmon surface, leading to a hypsochromic shift; and (*ii*) it's not possible to confirm derivatization by the LSPR shifting since the *Calendula officinalis* extract's spectra have a clear "shoulder" at λ = 495 nm, and it could be overlapping with the LSPR "unshifted" at 520 nm. In this case, the convolute peak is expected to be at 510 nm. From the abovementioned, there is little evidence yet to confirm an effective conjugation of AuNP with the carotenoids contained in the *Calendula officinalis*.

To confirm the functionalization, DLS and ELS measurements were also performed.

Dynamic light scattering

Through DLS analysis, the hydrodynamic diameter (d_h) of a particulate system dispersed in a continuous phase can be determined.[63] In this case, this refers to the AuNP-Cit and AuNP-Cale colloids in aqueous solution.

It is important to note that this technique is based on light scattering physics described by the "Tyndall Effect", so it is highly sensitive to nanoparticle diameter ($I \alpha d^6$).[64-66] Consequently, the intensity distribution plot $I = f(d)$ oversize the presence of larger AuNPs due to the sixth-power dependence of intensity. In addition, even a small minority of simple aggregates will be disproportionately represented in this graph (Figure 4, left). Taking the previous in mind, one could argue that there are two groups of AuNP-Cale synthesized with hydrodynamic diameters of d_h = (26 ± 3) nm and d_h = (122 ± 13) nm, which, as stated above is an overrepresentation of the fraction of AuNP-Cale aggregates.

For this reason, the number distribution plot $N = f(d)$ is also generated, as it indicates the majority population based on corrections applied to the autocorrelation function using known optical parameters theoretically derived from Mie equation.[67,68] (Figure 4, right).

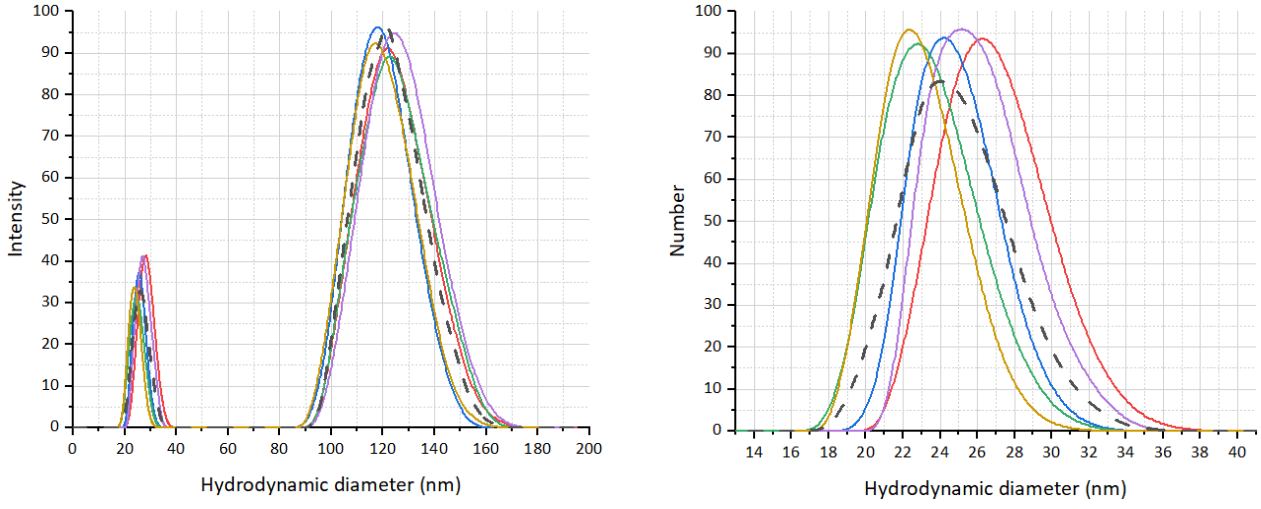

Figure 4. Intensity (left) and number (right) distribution as a function of hydrodynamic diameter of particles in suspension. Solid lines represent individual measurements (n = 6) and the dashed line corresponds to the average curve of all measurements.

Altogether, from the $N = f(d)$ graph, a hydrodynamic diameter of d_h = (25 ± 3) nm, with a PDI of 0.29 ± 0.01 was determined, in accordance with the d_h obtained for the small diameter group in the $I = f(d)$ graph in Figure 4, left. The same procedure was followed for AuNP-Cit, obtaining from $N = f(d)$ to d_h = (19 ± 3) nm (Figure SM-2).

These results show an increment by approximately 10 nm in the AuNP-Cit hydrodynamic diameter after derivatization procedure. DLS is highly sensitive to the presence of aggregates and changes in the hydration layer, so it cannot be assured that this increase is solely attributable to successful derivatization. If we were to consider this increase solely due to calendula adsorption, this growth was predicted by the following analysis: if it is assumed that the length of the functionalizing carotenoids is determined by lycopene, which is the longest carotenoid from the main three, involving 40 carbon atoms, of which 32 are sp^2 conjugated single and double bonds; that the average bond length is approximately 1.4 Å and that the molecule has its longer axis perpendicular to the AuNP surface; then it is expected the final diameter to grow d = 1.4 × 32 = 44.8 Å, each side of the sphere, so a total of roughly 89.6 Å ≈ 9 nm. Since citrate is such a small molecule, following the same reasoning, it is presumable that it provides only 1 nm per side to the AuNP core. In sum, the difference in d_h observed between AuNP-Cit and AuNP-Cale could be attributable to AuNP-Cit derivatization but need confirmation by other techniques.

Furthermore, the expected diameters of both AuNP-Cit and AuNP-Cale by transmission electron microscopy (TEM), should be in the range of 15 nm ≤ $d_{expected}$ ≤ 16 nm since this is the diameter of the AuNP core ($d_{expected} = d_h - 2.r_{ligand}$, where r_{ligand} is ligand longest axis length). To confirm these results AuNPs core diameter was measured by TEM.

Transmission electron microscopy

TEM measurements confirmed the AuNPs core diameter predicted by calculations based on the hydrodynamic diameter (d_h) determined by DLS.

For AuNP-Cit, TEM diameters (d_{TEM}) were determined for n = 372 individual AuNPs from 10 micrographs using FIJI software (Figure 5).

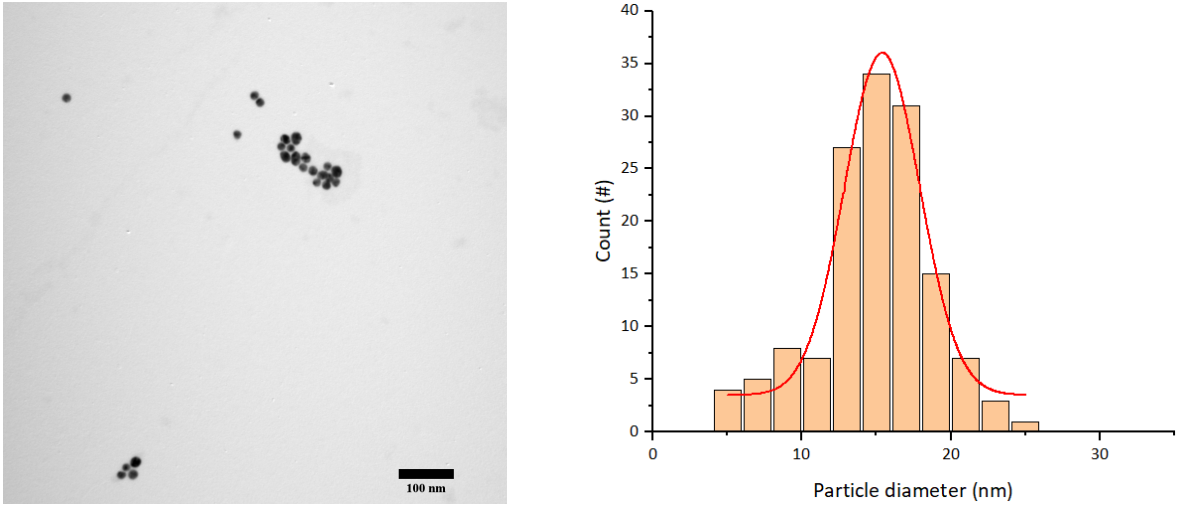

Figure 5. Left: TEM micrograph of citrate-reduced gold nanoparticles (AuNP-Cit) synthesized via the Turkevich method. The image shows spherical nanoparticles with varying degrees of aggregation. The scale bar indicates 100 nm. Right: Size distribution histogram of AuNP-Cit as a function of particle diameter. The synthesis resulted in particles with a diameter d_{TEM} = (16 ± 3). The discrete particles and small aggregates suggest successful formation of the desired colloidal gold system.

Random noise was manually diminished by outruling individuals AuNPs of areas less than A = 11 nm^2 (d_{TEM} < 4 nm) since they could be software artefacts from B&W noise in the picture. The presence of aggregates in some micrographs made individual nanoparticle measurement difficult, so they were excluded by applying a circularity threshold higher than 0.8 and restricting the area to less than 3000 nm^2. On doing so, a population of n = 253 individuals with the distribution presented in Figure 5 (right) was obtained.

The TEM size distribution analysis revealed a unimodal population distribution, with the majority of particles centered at approximately 16 nm and a minor subpopulation observed around 35 nm. These observations are consistent with the high polydispersity index obtained from dynamic light scattering (DLS) measurements, indicating significant heterogeneity in the sample's size distribution. From the gaussian fitting of the count graph for majority population, a diameter of d_{TEM} = (16 ± 3) nm was obtained. In accordance with $d_{expected}$, predicted from the d_h measured by DLS for both AuNP-Cit and AuNP-Cale.

Electrophoretic light scattering

The ζ-potential of a NP solution (diffuse layer potential) gives an idea of the surface charge of the NP and, therefore, of its stability (in terms of the interactions that keep the solid species dispersed in a homogeneous medium).[69]

It is considered that surface charges ζ-potential > 30 mV or ζ-potential < 30 mV are sufficient to overcome the weak attractive interactions between the dispersed particles in the homogeneous phase, so that NP whose ζ-potential meet the previous requirement are considered a stable NP colloidal suspension.

Considering the above, 12 ELS tests were carried out, obtaining a ζ-potential = (-52 ± 2) mV, indicating that the AuNP-Cit are stable under the working conditions (pH = 5 and T = 25 ºC).

In comparison, the ζ-potential obtained for the AuNP-Cale was ζ-potential = (-2 ± 6) mV, suggesting that the carotenoids of the *C. officinalis* extract displaced the citrates on the AuNP surface. Since those carotenoids are not charged, compared to citrate groups at pH 5—where two of three citrate carboxylic acid groups are ionized—if the derivatization is successful, it is expected to be a diminishment to round zero ζ-potential, from citrate to carotenoids, just as our results show.

Previously, ζ-potential was associated with the electrostatic repulsion forces needed for stable NP colloidal suspension. So, it is clear that AuNP-Cale does not fulfil this requirement. Thus, assessing a colloidal stability assay is mandatory to analyze how this diminishment in ζ-potential affected NP stability.

Colloidal stability assay

Colloidal stability was followed by spectrophotometry in the visible range at wavelengths of 520 nm (LSPR maxima), 650 nm plasmonic coupling's bathochromic shifts and 455 nm (maximum absorption of carotenoids, Figure 2). No changes were observed at 455 nm regarding increasing NaCl concentration (data not shown).

It was detected an increase in the critical concentration of NaCl (the concentration at which half of the NPs are aggregated) from $[NaCl]_c$ = (22 ± 2) mM for AuNP-Cit to $[NaCl]_c$ = (61 ± 1) mM for AuNP-Cale (Figure 6).

From this result, it is confirmed that, apart from having successfully achieved the functionalization of AuNP with carotenoids from *C. officinalis*, the same improves their stability, in contrast of what was expect by ELS measurements.

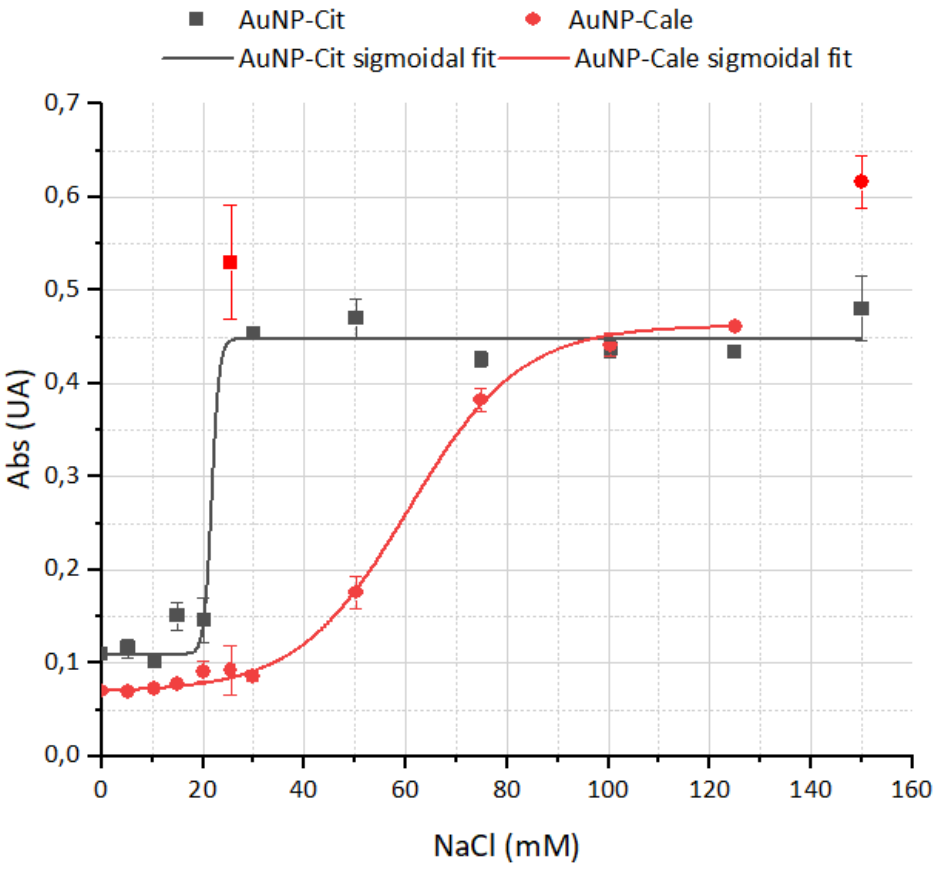

Figure 6. AuNP-Cit and AuNP-Cale colloidal stability assay, followed by UV-Vis spectrophotometry at 650 nm.

This apparent contradiction can be explained since the structure of carotenoids could provide extra steric stabilization that prevents nanoparticles from approaching each other, even when electrostatic repulsion is minimal. Also, carotenoids possess hydrophobic regions (polyene chains) and polar groups (hydroxyl groups in flavoxanthin and lutein). In this sense, interaction between hydrophobic groups of carotenoids (mainly Van der Walls interactions), and hydrophilic interactions between carotenoids and the solvent (hydrogen bonds and dipole mediated interactions) allow them to organize on the surface of NPs forming an effective protective layer.

In summary, Table I presents the key physicochemical parameters obtained for AuNP-Cit and AuNP-Cale, and the combined evidence from multiple characterization techniques demonstrates successful functionalization.

Table I. Comparative physicochemical characterization of AuNP-Cit and AuNP-Cale

Parameter	AuNP-Cit	AuNP-Cale	Change
λ_{LSPR} (nm)	519	510	- 9 nm
d_h (nm)	19 ± 3	25 ± 3	+ 6 nm
d_{TEM} (nm)	16 ± 3	16 ± 3	No change observed
ζ-potential (mV)	- 52 ± 2	- 2 ± 6	+ 50 mV
Colloidal stability against [NaCl] (mM)	22 ± 2	61 ± 1	+ 39 mM

Then, to further evaluate the nature of the functionalization, cyclic voltammetry studies were conducted.

Cyclic voltammetry

Voltammetric profiles for FTO/TiO_2 electrodes were recorded for the solutions containing AuNP-Cit, Cale, or AuNP-Cale in the supporting electrolyte. Distinct differences were observed, highlighting interesting variations in the redox behavior of the analyzed species (Figure 7).

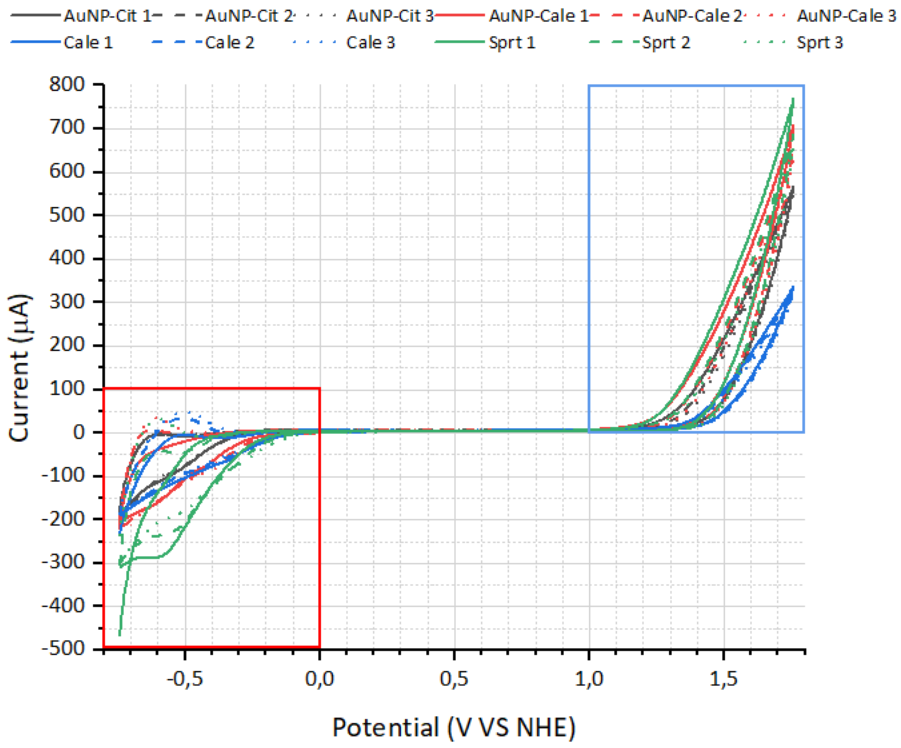

Figure 7. Voltammetric profiles recorded using FTO/TiO_2 electrodes for different analytes in the supporting electrolyte 0.1 M $NaClO_4$:EtOH (1:1) (Sprt, green lines), citrate reduced gold nanoparticles (AuNP-Cit, black lines), gold nanoparticles functionalized with *C. officinalis* extract (AuNP-Cale, red lines) and *C. officinalis* extract (Cale, blue lines). Scan rate: 50 mVs^{-1}. Straight, dashed and dotted lines correspond to the first, second and third voltammetric scans respectively.

As deduced from the voltammetric profiles, two main redox processes were detected for all the evaluated samples: an anodic contribution at ca. 1.5 V and a redox species at ca. -0.6 V (a cathodic contribution and, after cycling, a related anodic peak appeared). The oxidation peak at ca. 1.5 V could be ascribed to the -OH oxidation. Regarding the species at ca. -0.6 V, the cathodic and anodic peaks are ascribed to a process involving allylic oxygen, found in the carotenoids from AuNP-Cale and Cale, but not present in AuNP-Cit, as reported.[70,71]

To further analyze this voltammogram, Figure 8 zooms in on the red and blue windows in Figure 7.

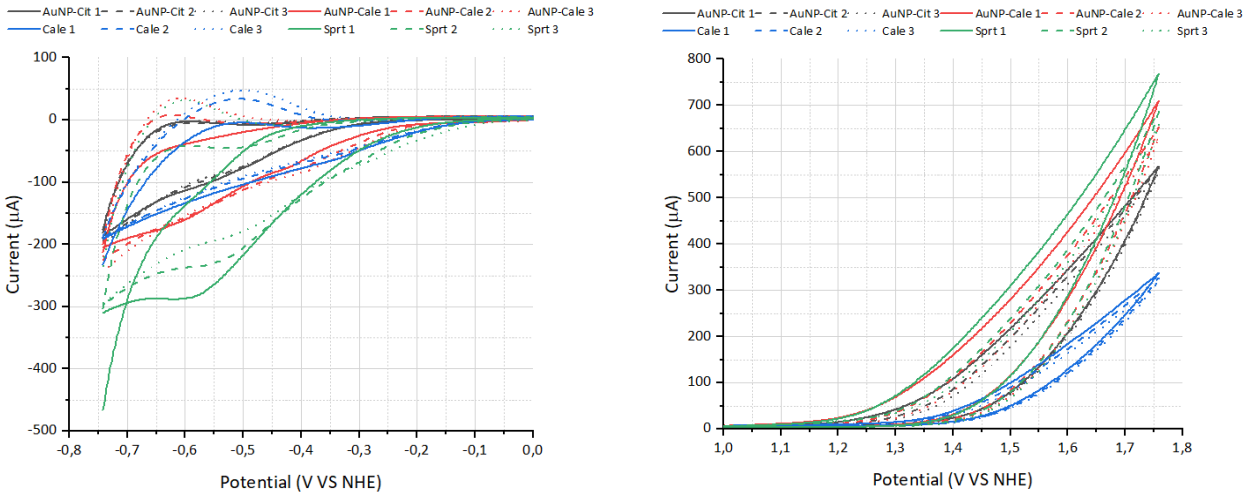

Figure 8. Voltammetric profiles recorded using FTO/TiO_2 electrodes for different analytes in the supporting electrolyte 0.1 M $NaClO_4$:EtOH (1:1). Zoomed from red window (left) and blue window (right) in Figure 7, colors and lines are as in the figure mentioned.

From Figure 8 (left), it is observed that profiles recorded within the -0.75 to 0.0 V range in the presence of AuNP-Cit show no discernible differences, i.e., the area, potential and shape are the same for the three potential scans. On the contrary, voltammetric profiles recorded from Cale solutions showed progressively increasing areas in every cycle. This behavior can be attributed to the electrochemical activity of carotenoids present in *Calendula officinalis* extract.[70] During the first cycle, electroactive carotenoids undergo redox reactions at the electrode surface allowing the adsorption of the involved species, which leads to a partial passivation of the electrode surface. This passivation subsequently increases the capacitive current in the following cycles, resulting in larger areas for the intensity current peaks. The progressive increase in area with each cycle suggests that this passivation process continues incrementally as more carotenoids interact and adsorb onto the electrode surface. The same behaviour is observed in the presence of AuNP-Cale conjugate, suggesting that the derivatization was successful and that the gold nanoparticles are, at least, partially covered with *Calendula officinalis* extract.

In addition, the anodic intensity current peaks were found at -0.65 V for AuNP-Cale, whereas are detected at -0.50 V for Cale alone. It could be argued, that besides the AuNP-Cit peaks have very small currents, their dI/dV = 0 values are closest to AuNP-Cale that to Cale alone. In this sense, it is suggested that the voltammogram corresponds to a different entity than both above-mentioned.

Thus, AuNP-Cale is a well-functionalized AuNP with *Calendula officinalis* extract, according to these voltammetric results. This conclusion is supported by both panels of Figure 8.

Following all the observations arising from the voltammetric measurements, it can be highlighted that: (1) profiles and features related to the redox behaviour coming from Cale extracts differ significantly from those observed when linked to the AuNP; (2) redox behaviour recorded in the presence of AuNP-Cit is different from that observed for AuNP-Cale; and (3) when AuNP-Cale solutions are evaluated, the voltammetric profiles significantly differs from those arose using pure Cale solutions. Then, conjugation between AuNP-Cit and Cale could be confirmed. The stability of the AuNP-Cale is good enough to support the application of different potential routines.

Technological evaluation of AuNP-Cale

AuNP-Cale as a dye-sensitized solar cell sensitizer

Having confirmed the successful functionalization of gold nanoparticles with *Calendula officinalis* extract through comprehensive physicochemical and electrochemical characterization, we next explored the potential technological application of this nanoconjugate as a sensitizer for DSSC.

To evaluate AuNP-Cale as a sensitizer, cells containing Cale, AuNP-Cit and AuNP-Cale were assembled. Cale was also used in a co-adsorption procedure, and AuNP-Cit was added in a sequential step. Measurements using citrate as sensitizer were taken as a blank experiment.

The performance of each configuration was evaluated through current-voltage measurements under simulated solar illumination (Table II) and electrochemical impedance spectroscopy in darkness (Table III).

Table II. Photovoltaic properties of cells assembled with different sensitizers. All measurements were performed under one sun light intensity of 100 mW cm^{-2}, AM 1.5 G and the active areas were 0.36 cm^2 for all the cells. J_{SC} is the short-circuit current density, V_{OC} the open circuit potential, FF is the fill factor and η is the power conversion efficiency (PCE). Average values coming from at least three independent assembled cells.

Dye	η (%)	FF	V_{oc} (V)	J_{sc} (A cm^{-2})
Cale	0.020	0.36	0.24	2.2 10^{-4}
AuNP-Cale	0.012	0.35	0.20	1.7 10^{-4}
AuNP-Cit	0.019	0.33	0.30	1.8 10^{-4}
Cale + AuNP	0.040	0.39	0.28	7.2 10^{-4}
Citrate	0.027	0.45	0.42	1.4 10^{-4}

Some facts can be deduced from the measured results. Firstly, when applied as a sensitizer, the conjugated AuNP-Cale did not improve the DSSC performance. The reason is that the conjugate split in the components, also considering that the photoanode prior to the cell's assembly is pink-coloured and became colourless after 60 min inside the DSSC (i.e., in contact with the electrolyte solution). This makes sense since the carotenoids and xanthophylls of the cell extract possess only a few OH groups that can interact with the AuNP or the TiO_2. Then, when conjugated AuNP-cale are added to the FTO/TiO_2 photoanode, cale is adsorbed onto the semiconductor involving the same functional groups bonded to the AuNP. Nevertheless, the efficiency improvement was measured when adding the AuNP-Cit to the FTO/TiO_2/Cale electrode. In this case, the cell's performance is probably related to a better electrode surface coverage. When compounds of the cale extract adsorbed to the semiconductor, some surface patches remained uncovered. Then, those areas could be covered by the added AuNP-Cit, improving the electrode transference between dyes and the semiconductor and, therefore, increasing the cell's efficiency.

From the electrochemical impedance spectroscopy measurements, characteristic times of the cell were determined (Table III). As previously reported, transmission line-based model was employed to fit the measured profiles.

Table III. Values obtained from fitting the experimental data measured at V = 0.45 V, in darkness, using a transmission line-based model. Γt is the time constant for the transport of the injected electrons that diffuse through the nanoparticle network (calculated as Γt = Rt × Cμ, with Cμ, the chemical capacitance at the TiO_2/dye/electrolyte interface associated with the variation in the electron density and the displacement of the Fermi level); Γrec, the recombination time that reflects the lifetime of an electron in the photoanode (calculated as Γrec = Rct × Cμ).

	AuNP-Cit	Cale + AuNP-Cit sequential	Cale
Γrec = Rct x Cμ / s	0.057	0.0200	0.0120
Γt = Rt x Cμ / s	0.011	0.0007	0.0002

The performances of the DSSCs have to be explained by the differences in the time-constant values. For this reason, DSSCs sensitized with AuNP-Cit are among the worst measured, because of their high Γt. In addition, DSSCs showed high Γrec values, which is essential to ensure an acceptable cell's efficiency.

As expected, more efficient cells are those with lower Γt times and higher Γrec ones. For the evaluated cells, these facts are shown for DSSC sensitized with a mixture of the extracted dye followed by the addition of AuNP. This is in agreement with our previous studies, where we reported the application of silver nanoparticles as co-adsorbents improves DSSC performance, highlighting the importance of achieving greater surface coverage to reduce direct electron transfer between the TiO_2 and the redox couple of the electrolyte.[72]

Infrared spectroscopy

IR spectra were taken to determine if conjugation was achieved by covalent bonding or by Van der Walls interactions. Also, to determine if the DSSCs were sensitized with the dye and/or with the AuNP-Cale conjugate.

Figure 9 shows the spectra of AuNP-Cit, AuNP-Cale and Cale alone, before sensitization. In parallel, Figure 10 shows AuNP-Cit, AuNP-Cale and Cale with and without TiO_2.

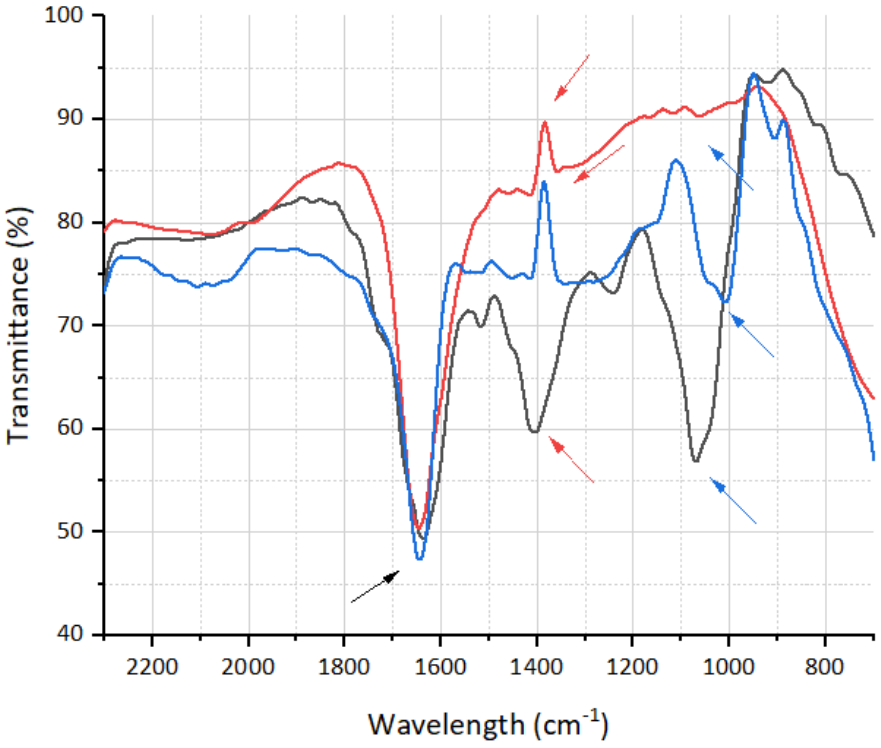

Figure 9. FTIR spectra of AuNP-Cit (black line), AuNP-Cale (red line), and Cale (blue line) in the 700-2300 cm^{-1} region. Black arrow indicates COO^- asymmetric stretching, red arrows indicate COO^- symmetric stretching, and blue arrows indicate C-OH stretching.

From Figure 9, the main absorption band appreciated has its minimum centered in $\tilde{\upsilon}$ = 1645 cm^{-1} (black arrow), which corresponds to both COO^- asymmetric stretching (from the citrate of AuNP-Cit). It is well established that the asymmetric COO^- stretching occurs at $\tilde{\upsilon}$ = 1715 cm^{-1} and the inductive effect on the stretching environment provokes shifting towards lower energies,[73] as seen in the spectra. Also, the C=C stretching energy from polyenes (like those from the main carotenoids presented in Figure 1) occurs at the abovementioned wavenumber. The next evident peak, which minimum is centered at $\tilde{\upsilon}$ = 1405 cm^{-1} (red

arrows), corresponds to the symmetric stretching of COO^-, which was observed only in the AuNP-Cit as expected. The last distinctive peak observed, which occurs at $\tilde{u}$ = 1070 cm^{-1} (blue arrows), corresponds to the C-O stretching of alcohols (as those from the citrate in AuNP-Cit). In the case of Cale, the C-O from the carotenoids shown in Figure 1 (except lycopene) have a different environment than those from the citrate. In addition, the extensive network of conjugated double bonds may affect the whole structure's electronic distribution, consequently lowering the vibration energy towards a wavenumber of $\tilde{u}$ = 1000 cm^{-1}. Here, it is proposed that the C-O that were forming C-OH bonds are now involved in the coordination with the gold nanoparticle surface (C-O-Au), which may lower the energies out of the spectra, diminishing its intensity until it is undetectable.

Some significant differences are observed when AuNP-Cit is compared with TiO_2/AuNP-Cit (AuNP-Cit after derivatization, Figure 10-a). The main difference is that AuNP-Cit shows deeper minima in the regions of approximately $\tilde{u}$ = 1400 cm^{-1} (Figure 9, red arrows) and $\tilde{u}$ = 1070 cm^{-1} (Figure 9, blue arrows). In parallel, TiO_2/AuNP-Cit presents a flatter profile in the mentioned region. Regarding the region of $\tilde{u}$ = 1645 cm^{-1} (corresponding to COO^- asymmetric stretching Figure 9, black arrow), it could be argued that this vibrational mode wasn't affected by TiO_2 sensibilization. On the other hand, symmetric stretching of COO^-, which is observed around $\tilde{u}$ = 1400 cm^{-1} was appreciably diminished after derivatization, suggesting coordination of COO^- with both TiO_2 and Au, causing the restriction of that particular vibration. Finally, the practically disappearing of the $\tilde{u}$ = 1070 cm^{-1} minima (corresponding to C-OH stretching of the citrate) suggests the place for bonding formation between AuNP-Cit and TiO_2, probably Au-$O_{(COOH)}$-C-$O_{(COH)}$-Ti, where $O_{(COOH)}$ corresponds to carboxylate oxygen, and $O_{(COH)}$ corresponds to the alcohol oxygen.

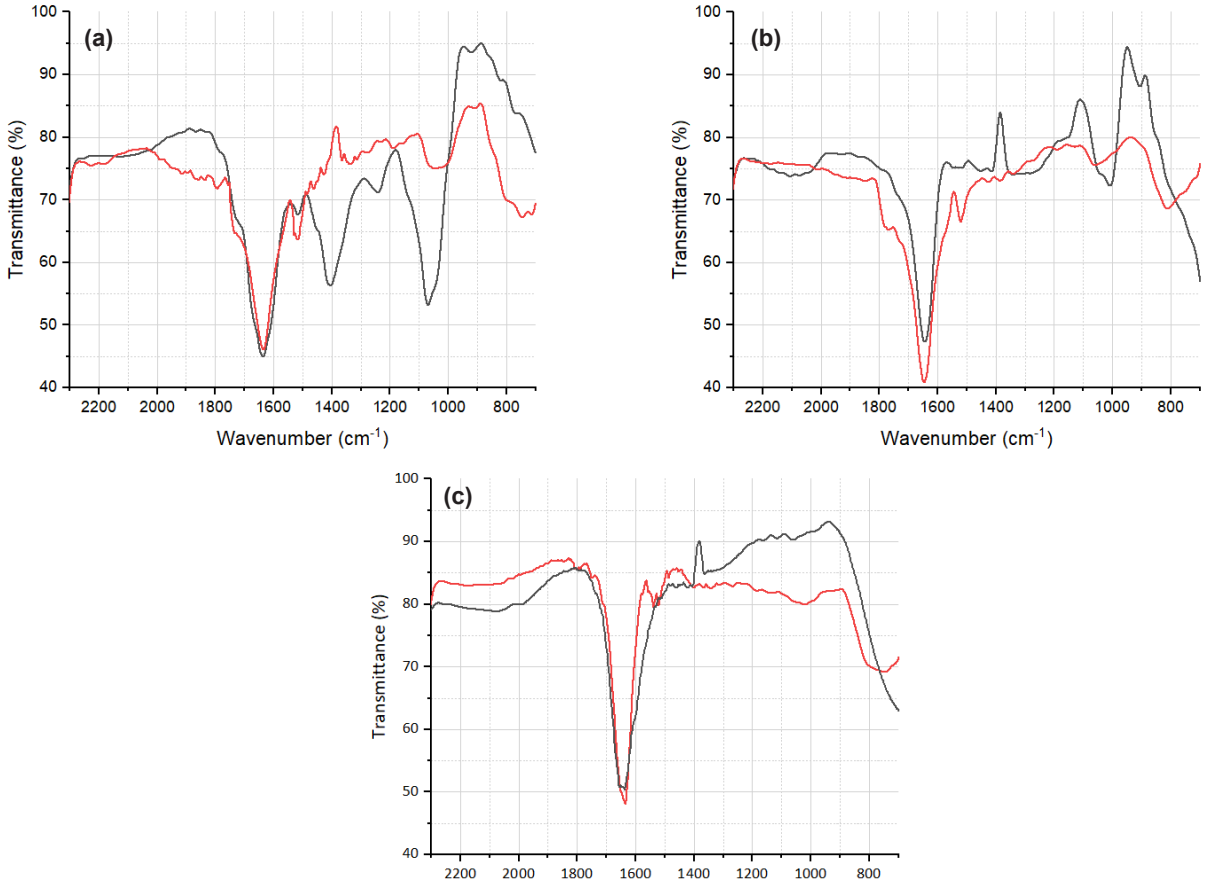

Figure 10. FTIR spectra of AuNP-Cit (a), Cale (b) and AuNP-Cale (c) alone (black lines) and adsorbed onto TiO_2 (red lines).

When Cale is compared with TiO_2/Cale (Cale after derivatization, Figure 10-b), the differences observed are comparable to those between Cale and AuNP-Cale. It is proposed that the hydroxyl and carbonyl groups of carotenoids appear to form coordination bonds with the TiO_2 surface, as they did with the gold nanoparticles, as evidenced by a general flattening of the spectrum and a decrease in the intensity of characteristic OH and C-O-C peaks.

No significant changes are observed when AuNP-Cale is compared with TiO_2/AuNP-Cale (AuNP-Cale after derivatization, Figure 10-c). Following the above reasoning, carotenoids from *Calendula officinalis* are now bonded to the gold nanoparticle, to the TiO_2 or both, being FTIR spectroscopy insufficient to conclude in this sense firmly. Because of this reason, FORS was performed as follows.

Fiber optic reflectance spectroscopy

FORS was performed for dyes adsorbed onto the TiO_2 before and after the DSSC was assembled, specifically before and after immersion in the iodine-based electrolyte used in the assembled cells (Figure 11). In all evaluated cases, absorbance profiles were improved after contacting the iodine-based solutions, probably due to the desorption of molecules attached to the TiO_2 surface through weak bondings. For samples measured before the DSSC built-up, it is appreciable that AuNP-Cale spectra are the sum of both AuNP-Cit and Cale spectra. AuNP-Cit and AuNP-Cale have their maxima of 520 and 540 nm, respectively, as expected from the LSPR position.

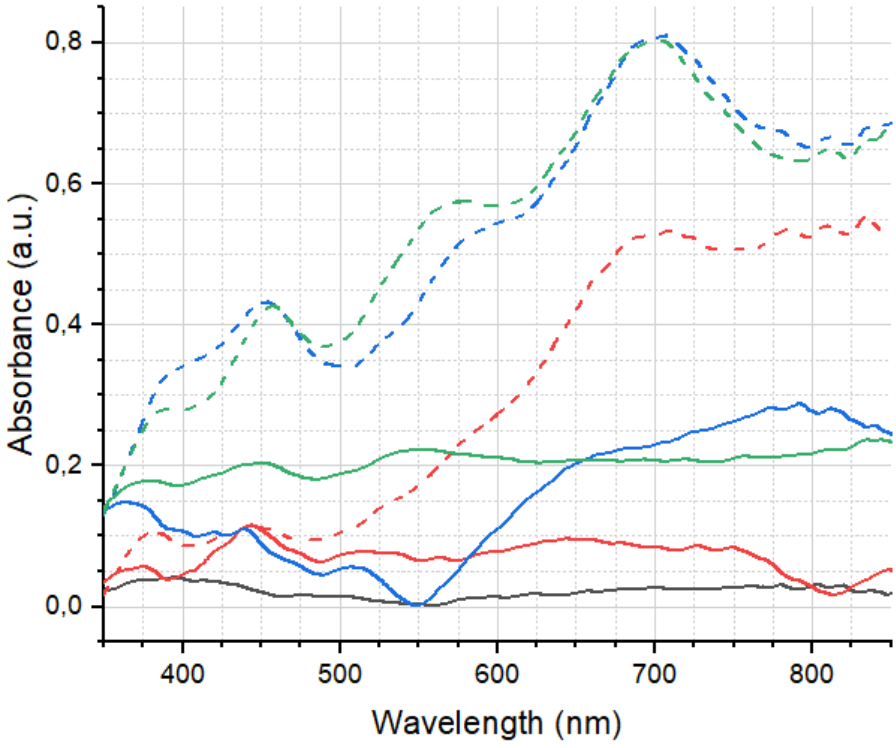

Figure 11. UV-Vis reflectance spectra of AuNP-Cit (red line), Cale (blue line) and AuNP-Cale (green line) before and after DSSC assembly (straight and dashed lines respectively) in the visible 350-850 nm range.

However, some features changed after the DSSC assembly and getting in contact with the iodine-based solutions. Spectra for Cale and AuNP-Cale are almost identical.

This is in line with what was observed when evaluating the DSSC: cells sensitized with the conjugate AuNP-Cale showed a similar power conversion efficiency to those sensitized with the components separated. Figure 11 shows that in all cases studied, absorbance profiles were improved after getting in contact with

the iodine-based solutions, probably to desorption of molecules attached to the TiO_2 surface through weak bonding. When attached to the TiO_2, carotenoids involved the same functional groups that bond the AuNP. Therefore, the conjugate is split into the elements, as confirmed by the reflectance spectra measured after the cell's evaluation.

CONCLUSIONS

Calendula officinalis extract was evaluated as a functionalization agent for gold nanoparticles (AuNPs), using citrate-reduced AuNPs (AuNP-Cit) as a reference. The resulting nanoconjugate, AuNP-Cale, underwent comprehensive characterization using DLS, ELS, colloidal stability assay, TEM, and spectroscopy.

Functionalization was confirmed by increased hydrodynamic diameter and reduced zeta potential of AuNP-Cale compared to AuNP-Cit. Despite the reduced zeta potential, the AuNP-Cale showed improved colloidal stability, which was attributed to the potential steric stabilization provided by the carotenoids in the extract. Voltammetry, FTIR and FORS analyses further supported the successful derivatization and possible interactions with the AuNP and TiO_2 surfaces.

AuNP-Cale was then explored as a sensitizer for DSSCs. While pre-formed AuNP-Cale did not enhance DSSC efficiency when applied directly, improved performance was achieved when AuNP-Cit was added sequentially after the *C. officinalis* extract on the TiO_2 electrode. This enhanced performance correlated with improved light absorption (FORS) and favorable EIS parameters, likely resulting from better electrode coverage achieved by the sequential deposition method.

Conflicts of interest

The authors have no known competing financial interests or personal relationships that could have appeared to influence the work reported in this paper.

Acknowledgements

Pablo Fagúndez and María Fernanda Cerdá are SNI-ANII (Agencia Nacional de Investigación e Innovación) and PEDECIBA (Programa de Desarrollo de las Ciencias Básicas) researchers.

REFERENCES

(1) Feynman, R. P. There's Plenty of Room at the Bottom. *Eng. Sci.* **1959**, *5* (23), 22–36.
(2) Laurent, S.; Forge, D.; Port, M.; Roch, A.; Robic, C.; Vander Elst, L.; Muller, R. N. Magnetic Iron Oxide Nanoparticles: Synthesis, Stabilization, Vectorization, Physicochemical Characterizations, and Biological Applications. *Chem. Rev.* **2010**, *110* (4), 2574–2574. https://doi.org/10.1021/cr900197g
(3) Loureiro, A.; Azoia, N. G.; Gomes, A. C.; Cavaco-Paulo, A. Albumin-Based Nanodevices as Drug Carriers. *Curr. Pharm. Des.* **2016**, *22* (10), 1371–1390. https://doi.org/10.2174/1381612822666160125114900
(4) Martis, E.; Badve, R.; Degwekar, M. Nanotechnology Based Devices and Applications in Medicine: An Overview. *Chron. Young Sci.* **2012**, *3* (1), 68. https://doi.org/10.4103/2229-5186.94320
(5) Nikalje, A. P. Nanotechnology and Its Applications in Medicine. *Med. Chem.* **2015**, *5* (2). DOI: 10.4172/2161-0444.1000247
(6) Todescato, F.; Fortunati, I.; Minotto, A.; Signorini, R.; Jasieniak, J.; Bozio, R. Engineering of Semiconductor Nanocrystals for Light Emitting Applications. *Materials* **2016**, *9* (8), 672. https://doi.org/10.3390/ma9080672
(7) Dong, H.; Wen, B.; Melnik, R. Relative Importance of Grain Boundaries and Size Effects in Thermal Conductivity of Nanocrystalline Materials. *Sci. Rep.* **2014**, *4* (1), 7037. https://doi.org/10.1038/srep07037
(8) Ma, E. Controlling Plastic Instability. *Nat. Mater.* **2003**, *2* (1), 7–8. https://doi.org/10.1038/nmat797
(9) Ripp, S.; Henry, T. B. (Eds.) *Biotechnology and Nanotechnology Risk Assessment: Minding and Managing the Potential Threats around Us*. American Chemical Society Publications, Washington, DC, 2011, Vol. 1079. https://doi.org/10.1021/bk-2011-1079

(10) Golobič, M.; Jemec, A.; Drobne, D.; Romih, T.; Kasemets, K.; Kahru, A. Upon Exposure to Cu Nanoparticles, Accumulation of Copper in the Isopod *Porcellio Scaber* Is Due to the Dissolved Cu Ions Inside the Digestive Tract. *Environ. Sci. Technol.* **2012**, *46* (21), 12112–12119. https://doi.org/10.1021/es3022182
(11) Kosmala, A.; Wright, R.; Zhang, Q.; Kirby, P. Synthesis of Silver Nano Particles and Fabrication of Aqueous Ag Inks for Inkjet Printing. *Mater. Chem. Phys.* **2011**, *129* (3), 1075–1080. https://doi.org/10.1016/j.matchemphys.2011.05.064
(12) Holzinger, M.; Le Goff, A.; Cosnier, S. Nanomaterials for Biosensing Applications: A Review. *Front. Chem.* **2014**, *2*. https://doi.org/10.3389/fchem.2014.00063
(13) Millstone, J. E.; Kavulak, D. F. J.; Woo, C. H.; Holcombe, T. W.; Westling, E. J.; Briseno, A. L.; Toney, M. F.; Fréchet, J. M. J. Synthesis, Properties, and Electronic Applications of Size-Controlled Poly(3-Hexylthiophene) Nanoparticles. *Langmuir* **2010**, *26* (16), 13056–13061. https://doi.org/10.1021/la1022938
(14) Shaalan, M.; Saleh, M.; El-Mahdy, M.; El-Matbouli, M. Recent Progress in Applications of Nanoparticles in Fish Medicine: A Review. *Nanomedicine: Nanotechnology, Biology and Medicine* **2016**, *12* (3), 701–710. https://doi.org/10.1016/j.nano.2015.11.005
(15) Avasare, V.; Zhang, Z.; Avasare, D.; Khan, I.; Qurashi, A. Room-Temperature Synthesis of TiO_2 Nanospheres and Their Solar Driven Photoelectrochemical Hydrogen Production: Metal Organic Mediated Room Temperature Synthesis of TiO_2 Nanospheres. *Int. J. Energy Res.* **2015**, *39* (12), 1714–1719. https://doi.org/10.1002/er.3372
(16) Mueller, N. C.; Nowack, B. Exposure Modeling of Engineered Nanoparticles in the Environment. *Environ. Sci. Technol.* **2008**, *42* (12), 4447–4453. https://doi.org/10.1021/es7029637
(17) Ning, F.; Shao, M.; Xu, S.; Fu, Y.; Zhang, R.; Wei, M.; Evans, D. G.; Duan, X. TiO_2 /Graphene/NiFe-Layered Double Hydroxide Nanorod Array Photoanodes for Efficient Photoelectrochemical Water Splitting. *Energy Environ. Sci.* **2016**, *9* (8), 2633–2643. https://doi.org/10.1039/C6EE01092J
(18) Fang, X.-Q.; Liu, J.-X.; Gupta, V. Fundamental Formulations and Recent Achievements in Piezoelectric Nano-Structures: A Review. *Nanoscale* **2013**, *5* (5), 1716. https://doi.org/10.1039/c2nr33531j
(19) Gawande, M. B.; Goswami, A.; Felpin, F.-X.; Asefa, T.; Huang, X.; Silva, R.; Zou, X.; Zboril, R.; Varma, R. S. Cu and Cu-Based Nanoparticles: Synthesis and Applications in Catalysis. *Chem. Rev.* **2016**, *116* (6), 3722–3811. https://doi.org/10.1021/acs.chemrev.5b00482
(20) Li, Y.; Wang, H.; Feng, Q.; Zhou, G.; Wang, Z.-S. Gold Nanoparticles Inlaid TiO2 Photoanodes: A Superior Candidate for High-Efficiency Dye-Sensitized Solar Cells. *Energy Environ. Sci.* **2013**, *6* (7), 2156-2165. https://doi.org/10.1039/c3ee23971c
(21) Maojo, V.; García-Remesal, M.; De La Iglesia, D.; Crespo, J.; Pérez-Rey, D.; Chiesa, S.; Fritts, M.; Kulikowski, C. A. Nanoinformatics: Developing Advanced Informatics Applications for Nanomedicine. In: Prokop, A. (Ed.). *Intracellular Delivery – Fundamentals and Applications*. Springer, Netherlands, Dordrecht, 2011, Vol. 5, pp 847–860. https://doi.org/10.1007/978-94-007-1248-5_26
(22) Maojo, V.; Fritts, M.; Martin-Sanchez, F.; De La Iglesia, D.; Cachau, R. E.; Garcia-Remesal, M.; Crespo, J.; Mitchell, J. A.; Anguita, A.; Baker, N.; et al. Nanoinformatics: Developing New Computing Applications for Nanomedicine. *Computing* **2012**, *94* (6), 521–539. https://doi.org/10.1007/s00607-012-0191-2
(23) Panneerselvam, S.; Choi, S. Nanoinformatics: Emerging Databases and Available Tools. *Int. J. Mol. Sci.* **2014**, *15* (5), 7158–7182. https://doi.org/10.3390/ijms15057158
(24) Brown, M. D.; Suteewong, T.; Kumar, R. S. S.; D'Innocenzo, V.; Petrozza, A.; Lee, M. M.; Wiesner, U.; Snaith, H. J. Plasmonic Dye-Sensitized Solar Cells Using Core−Shell Metal−Insulator Nanoparticles. *Nano Lett.* **2011**, *11* (2), 438–445. https://doi.org/10.1021/nl1031106
(25) Qi, J.; Dang, X.; Hammond, P. T.; Belcher, A. M. Highly Efficient Plasmon-Enhanced Dye-Sensitized Solar Cells through Metal@Oxide Core–Shell Nanostructure. *ACS Nano* **2011**, *5* (9), 7108–7116. https://doi.org/10.1021/nn201808g

(26) Jeong, N. C.; Prasittichai, C.; Hupp, J. T. Photocurrent Enhancement by Surface Plasmon Resonance of Silver Nanoparticles in Highly Porous Dye-Sensitized Solar Cells. *Langmuir* **2011**, *27* (23), 14609–14614. https://doi.org/10.1021/la203557f
(27) Nahm, C.; Choi, H.; Kim, J.; Jung, D.-R.; Kim, C.; Moon, J.; Lee, B.; Park, B. The Effects of 100 nm-Diameter Au Nanoparticles on Dye-Sensitized Solar Cells. *Appl. Phys. Lett.* **2011**, *99* (25), 253107. https://doi.org/10.1063/1.3671087
(28) Deepa, K. G.; Lekha, P.; Sindhu, S. Efficiency Enhancement in DSSC Using Metal Nanoparticles: A Size Dependent Study. *Sol. Energy* **2012**, *86* (1), 326–330. https://doi.org/10.1016/j.solener.2011.10.007
(29) Kawawaki, T.; Takahashi, Y.; Tatsuma, T. Enhancement of Dye-Sensitized Photocurrents by Gold Nanoparticles: Effects of Plasmon Coupling. *J. Phys. Chem. C* **2013**, *117* (11), 5901–5907. https://doi.org/10.1021/jp3120836
(30) Jeevanandam, J.; Barhoum, A.; Chan, Y. S.; Dufresne, A.; Danquah, M. K. Review on Nanoparticles and Nanostructured Materials: History, Sources, Toxicity and Regulations. *Beilstein J. Nanotechnol.* **2018**, *9*, 1050–1074. https://doi.org/10.3762/bjnano.9.98
(31) Yi, Z.; Zeng, Y.; Wu, H.; Chen, X.; Fan, Y.; Yang, H.; Tang, Y.; Yi, Y.; Wang, J.; Wu, P. Synthesis, Surface Properties, Crystal Structure and Dye-Sensitized Solar Cell Performance of TiO2 Nanotube Arrays Anodized under Different Parameters. *Results in Phys.* **2019**, *15*, 102609. https://doi.org/10.1016/j.rinp.2019.102609
(32) Korir, B. K.; Kibet, J. K.; Ngari, S. M. A Review on the Current Status of Dye-sensitized Solar Cells: Toward Sustainable Energy. *Energy Sci. Eng.* **2024**, *12* (8), 3188–3226. https://doi.org/10.1002/ese3.1815
(33) Javed, H. M. A.; Sarfaraz, M.; Nisar, M. Z.; Qureshi, A. A.; E Alam, M. F.; Que, W.; Yin, X.; Abd-Rabboh, H. S. M.; Shahid, A.; Ahmad, M. I.; Ullah, S. Plasmonic Dye-Sensitized Solar Cells: Fundamentals, Recent Developments, and Future Perspectives. *ChemistrySelect* **2021**, *6* (34), 9337–9350. https://doi.org/10.1002/slct.202102177
(34) Bohren, C. F.; Huffman, D. R. *Absorption and Scattering of Light by Small Particles*; A Wiley-Interscience publication. Wiley-CH Verlag GmbH & Co KGaA, New York, 2004. https://doi.org/10.1002/9783527618156
(35) Sepúlveda, B.; Angelomé, P. C.; Lechuga, L. M.; Liz-Marzán, L. M. LSPR-Based Nanobiosensors. *Nano Today* **2009**, *4* (3), 244–251. https://doi.org/10.1016/j.nantod.2009.04.001
(36) Jang, Y. H.; Jang, Y. J.; Kim, S.; Quan, L. N.; Chung, K.; Kim, D. H. Plasmonic Solar Cells: From Rational Design to Mechanism Overview. *Chem. Rev.* **2016**, *116* (24), 14982–15034. https://doi.org/10.1021/acs.chemrev.6b00302
(37) Zhou, J.; Ralston, J.; Sedev, R.; Beattie, D. A. Functionalized Gold Nanoparticles: Synthesis, Structure and Colloid Stability. *J. Colloid Interface Sci.* **2009**, *331* (2), 251–262. https://doi.org/10.1016/j.jcis.2008.12.002
(38) Vella, F. M.; Pignone, D.; Laratta, B. The Mediterranean Species *Calendula officinalis* and *Foeniculum vulgare* as Valuable Source of Bioactive Compounds. *Molecules* **2024**, *29* (15), 3594. https://doi.org/10.3390/molecules29153594
(39) Khalid, K.; da Silva, J. T. Biology of *Calendula officinalis* Linn.: Focus on Pharmacology, Biological Activities and Agronomic Practices. *Medicinal and Aromatic Plant Science and Biotechnology* **2012**, *6*, 12–27.
(40) Kurkin, V. A.; Sharova, O. V. Flavonoids from Calendula Officinalis Flowers. *Chem. Nat. Compd.* **2007**, *43* (2), 216–217. https://doi.org/10.1007/s10600-007-0084-3
(41) Komissarenko, N. F.; Chernobai, V. T.; Derkach, A. I. Flavonoids of Inflorescences of *Calendula officinalis*. *Chem. Nat. Compd.* **1988**, *24* (6), 675–680. https://doi.org/10.1007/BF00598181
(42) Muley, B.; Khadabadi, S.; Banarase, N. Phytochemical Constituents and Pharmacological Activities of Calendula Officinalis Linn (Asteraceae): A Review. *Trop. J. Pharm Res.* **2009**, *8* (5). https://doi.org/10.4314/tjpr.v8i5.48090

(43) Kishimoto, S.; Maoka, T.; Sumitomo, K.; Ohmiya, A. Analysis of Carotenoid Composition in Petals of Calendula (*Calendula officinalis* L.). *Biosci., Biotechnol., Biochem.* **2005**, *69* (11), 2122–2128. https://doi.org/10.1271/bbb.69.2122
(44) Hulkoti, N. I.; Taranath, T. C. Biosynthesis of Nanoparticles Using Microbes—A Review. *Colloids Surf., B* **2014**, *121*, 474–483. https://doi.org/10.1016/j.colsurfb.2014.05.027
(45) Durán, N.; Nakazato, G.; Seabra, A. B. Antimicrobial Activity of Biogenic Silver Nanoparticles, and Silver Chloride Nanoparticles: An Overview and Comments. *Appl. Microbiol. Biotechnol.* **2016**, *100* (15), 6555–6570. https://doi.org/10.1007/s00253-016-7657-7
(46) Tasic, L.; Stanisic, D.; Martins, L. G.; Cruz, G. C. F.; Savu, R. Insights of Green and Biosynthesis of Nanoparticles. In: Koduru, J. R.; Karri, R. R.; Mubarak, N. M.; Bandala, E. R. (Eds.). *Sustainable Nanotechnology for Environmental Remediation*, *Micro and Nano Technologies.* Elsevier, 2022. Chapter 3, pp 61–90. https://doi.org/10.1016/B978-0-12-824547-7.00020-5
(47) Baghizadeh, A.; Ranjbar, S.; Gupta, V. K.; Asif, M.; Pourseyedi, S.; Karimi, M. J.; Mohammadinejad, R. Green Synthesis of Silver Nanoparticles Using Seed Extract of *Calendula officinalis* in Liquid Phase. *J. Mol. Liq.* **2015**, *207*, 159–163. https://doi.org/10.1016/j.molliq.2015.03.029
(48) Wei, X.; Liu, Y.; El-kott, A.; Ahmed, A. E.; Khames, A. *Calendula officinalis*-based green synthesis of titanium nanoparticle: Fabrication, characterization, and evaluation of human colorectal carcinoma. *J. Saudi Chem. Soc.* **2021**, *25* (11), 101343. https://doi.org/10.1016/j.jscs.2021.101343
(49) Hao, W.; Jia, Y.; Wang, C.; Wang, X. Preparation, Chemical Characterization and Determination of the Antioxidant, Cytotoxicity and Therapeutic Effects of Gold Nanoparticles Green-Synthesized by *Calendula officinalis* Flower Extract in Diabetes-Induced Cardiac Dysfunction in Rat. *Inorg. Chem. Commun.* **2022**, *144*, 109931. https://doi.org/10.1016/j.inoche.2022.109931
(50) Santos, A. P.; Gonçalves, M. M.; Justus, B.; Fardin, D. P. D. S.; Toledo, A. C. O.; Budel, J. M.; Paula, J. P. D. *Calendula officinalis* L. flower extract-mediated green synthesis of silver nanoparticles under LED light. *Braz. J. Pharm. Sci.* **2022**, *58*, e19519. https://doi.org/10.1590/s2175-97902022e19519
(51) Fricano, A.; Tavormina, F.; Pignataro, B.; Vetri, V.; Ferrara, V. Progress and Prospects of Biomolecular Materials in Solar Photovoltaic Applications. *Molecules* **2025**, *30* (15), 3236. https://doi.org/10.3390/molecules30153236
(52) Turkevich, J. Colloidal Gold. Part II: Colour, Coagulation, Adhesion, Alloying and Catalytic Properties. *Gold Bull* **1985**, *18* (4), 125–131. https://doi.org/10.1007/BF03214694
(53) Turkevich, J.; Stevenson, P. C.; Hillier, J. A Study of the Nucleation and Growth Processes in the Synthesis of Colloidal Gold. *Discuss. Faraday Soc.* **1951**, *11*, 55. https://doi.org/10.1039/df9511100055
(54) Kimling, J.; Maier, M.; Okenve, B.; Kotaidis, V.; Ballot, H.; Plech, A. Turkevich Method for Gold Nanoparticle Synthesis Revisited. *J. Phys. Chem. B* **2006**, *110* (32), 15700–15707. https://doi.org/10.1021/jp061667w
(55) Méndez, E.; Fagúndez, P.; Sosa, P.; Gutiérrez, M. V.; Botasini, S. Experimental Evidences Support the Existence of an Aggregation/Disaggregation Step in the Turkevich Synthesis of Gold Nanoparticles. *Nanotechnology* **2021**, *32* (4), 045603. https://doi.org/10.1088/1361-6528/abbfd5
(56) Fagúndez, P.; Botasini, S.; Tosar, J. P.; Méndez, E. Systematic Process Evaluation of the Conjugation of Proteins to Gold Nanoparticles. *Heliyon* **2021**, *7* (6), e07392. https://doi.org/10.1016/j.heliyon.2021.e07392
(57) International Organization for Standardization (ISO). *Particle Size Analysis — Dynamic Light Scattering (DLS)*. ISO-22412:2017.
(58) Schindelin, J.; Arganda-Carreras, I.; Frise, E.; Kaynig, V.; Longair, M.; Pietzsch, T.; Preibisch, S.; Rueden, C.; Saalfeld, S.; Schmid, B.; et al. Fiji: An Open-Source Platform for Biological-Image Analysis. *Nat. Methods* **2012**, *9* (7), 676–682. https://doi.org/10.1038/nmeth.2019
(59) Botasini, S. Comparación del Tamaño de Nanopartículas de Oro Empleando Diferentes Técnicas y Protocolos de Medición. *INNOTEC* **2020**, No. 21, 10–24. https://doi.org/10.26461/21.02

(60) National Institute of Standards and Technology (NIST). Bonevich, J.; Haller, W. *Measuring the Size of Nanoparticles Using Transmission Electron Microscopy (TEM)*. NIST–Nanotechnology Characterization Laboratory (NCL) Joint Assay Protocol, PCC-X, Version 1.1, 2010. Gaithersburg, MD. Available at: https://tsapps.nist.gov/publication/get_pdf.cfm?pub_id=854083 (accessed: 10/2024)
(61) Abarca, C.; Ali, M. M.; Yang, S.; Dong, X.; Pelton, R. H. A Colloidal Stability Assay Suitable for High-Throughput Screening. *Anal. Chem.* **2016**, *88* (5), 2929–2936. https://doi.org/10.1021/acs.analchem.5b04915
(62) Britton, G.; Liaeen-Jensen, S.; Pfander, H. *Carotenoids: Handbook*. Birkhäuser Basel: Basel, 2004. https://doi.org/10.1007/978-3-0348-7836-4
(63) Stetefeld, J.; McKenna, S. A.; Patel, T. R. Dynamic light scattering: a practical guide and applications in biomedical sciences. *Biophys. Rev.* **2016**, *8* (4), 409–427. https://doi.org/10.1007/s12551-016-0218-6
(64) Tyndall, J. IV. On the blue colour of the sky, the polarization of skylight, and on the polarization of light by cloudy matter generally. *Proc. R. Soc. London* **1869**, *17*, 223–233. https://doi.org/10.1098/rspl.1868.0033
(65) Kerker, M.; Loebl, E. M. *The Scattering of Light and other Electromagnetic Radiation*. Elsevier Science, Saint Louis, 2016.
(66) Humzah, M. D. Tyndall, Rayleigh, Mei, and Raman scattering: Understanding their role in aesthetics. *Journal of Cosmetic Dermatology* **2024**, *23* (11), 3493–3496. https://doi.org/10.1111/jocd.16470
(67) Mie, G. “Beiträge zur Optik trüber Medien, speziell kolloidaler Metallösungen”. *Annalen der Physik* **1908**, *330* (3), 377–445. https://doi.org/10.1002/andp.19083300302
(68) Mishchenko, M. I. Gustav Mie and the fundamental concept of electromagnetic scattering by particles: A perspective. *J. Quant. Spectrosc. Radiat. Transfer* **2009**, *110* (14–16), 1210–1222. https://doi.org/10.1016/j.jqsrt.2009.02.002
(69) Xu, R. Electrophoretic Light Scattering / Zeta Potential Measurement. In: Scarlett, B. (Ed.). *Particle Characterization: Light Scattering Methods*. Springer Netherlands: Dordrecht, 2002, Chapter 6, pp 289–343. https://doi.org/10.1007/0-306-47124-8_6
(70) Čižmek, L.; Komorsky-Lovrić, Š. Study of Electrochemical Behaviour of Carotenoids in Aqueous Media. *Electroanalysis* **2019**, *31* (1), 83–90. https://doi.org/10.1002/elan.201800531
(71) Komorsky-Lovrić, Š. Voltammetry of Azobenzene Microcrystals. *J. Solid State Electrochem.* **1997**, *1* (1), 94–99. https://doi.org/10.1007/s100080050028
(72) Montagni, T.; Chialanza, M. R.; Cerdá, M. F. Blueberries as a Source of Energy: Physical Chemistry Characterization of their Anthocyanins as Dye-Sensitized Solar Cells’ Sensitizers. *Solar* **2023**, *3* (2), 283–297. https://doi.org/10.3390/solar3020017
(73) Silverstein, R. M.; Webster, F. X.; Kiemle, D. J. *Spectrometric Identification of Organic Compounds*, 7th ed. John Wiley & Sons: Hoboken, NJ, 2005.

SUPPLEMENTARY MATERIAL

Carotenoid concentration calculation

According to Britton, G. et al. 2004 (reference No. 62 in the article), the molar absorption coefficient of carotenoids can be estimated using Equation (1):

$$\varepsilon = \left(A^{1\%} \times molecular\ weight\right)/10 \qquad \text{Equation (1)}$$

Where $A^{1\%}$ is defined as the theoretical absorbance of a solution of 1% (w/v) concentration in a cuvette with a path length of b = 1 cm.

According to Kishimoto, S. et al. 2005 (reference No. 43 in the article), the main carotenoids present in *Calendula officinalis* are flavoxanthin (28.5 %), luteoxanthin (11.0 %) and lycopene (8.7 %). Taking these carotenoids as the only components in the sample (normalized to 100%), these percentages become 59.1%, 22.8%, and 18.1% for flavoxanthin, luteoxanthin, and lycopene, respectively. From the handbook previously mentioned (reference No. 62 in the article), $A^{1\%}$ at the absorption maxima of these carotenoids were found to be:

$$A^{1\%}_{Lycopene} = 3450,\ A^{1\%}_{Flavoxanthin} = 2570,\ \text{and}\ A^{1\%}_{Luteoxanthin} = 2940$$

The molecular weights of these carotenoids are:
$MW_{Lycopene}$ = 536 g mol^{-1}, $MW_{Flavoxanthin}$ = 568 g mol^{-1} and $MW_{Luteoxanthin}$ = 568 g mol^{-1}

Applying Equation (1), the absorption coefficients are:

$\varepsilon_{Lycopene}$ = (3450 × 536)/10 = 184,920 L mol^{-1} cm^{-1}
$\varepsilon_{Flavoxanthin}$ = (2570 × 568)/10 = 145,976 L mol^{-1} cm^{-1}
$\varepsilon_{Luteoxanthin}$ = (2940 × 568)/10 = 166,992 L mol^{-1} cm^{-1}

Meanwhile, applying the additivity property of absorptivity, the mixture coefficient is:

$\varepsilon_{mix} = \sum(xi \times \varepsilon_i)$.

So, for *C. officinalis* it is:

ε_{cale} = (0.591×145,976) + (0.228 × 166,992) + (0.181 × 184,920) = 157,817 L mol^{-1} cm^{-1}

Once the ε_{cale} was determined, carotenoids concentration in *Calendula officinalis* determination is trivial, by the *Bouguer-Lambert-Beer's Law*, in this sense:

For 1E extraction:

A_1 = 0.6311 × 50 = 31.555, [Carotenoid] = 31.555 / (157,817 × 1) = 0,000199947 M

A_2 = 1.0074 × 30 = 30.222, [Carotenoid] = 30.222 / (157,817 × 1) = 0,0001915 M

The, 1E extraction concentration is [Carotenoid] = (0,196 ± 0,006) mM

Analogously, for 2E extraction:

A_1 = 0.6951 × 100 = 69.51, [Carotenoid] = 69.510 / (157,817 × 1) = 0,000440447 M

A_2 = 1.3395 × 50 = 69.975, [Carotenoid] = 69.975 / (157,817 × 1) = 0,000443393 M

The, 2E extraction concentration is [Carotenoid] = (0,442 ± 0,002) mM

AuNP-Cit UV-Vis spectra

AuNP-Cit UV-Vis spectra were taken in serial dilutions. The LSPR position was determined by taking the point where the derivative of $d_{Abs}/d\lambda = 0$ (curve maxima).

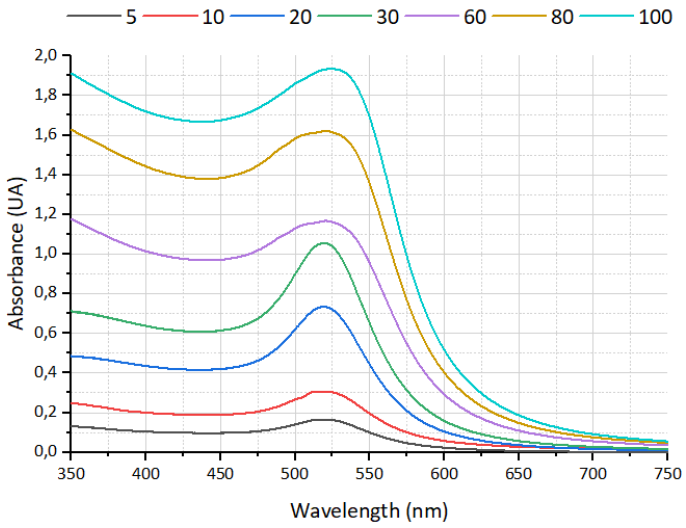

Figure SM-1. AuNP-Cit absorbance spectra in serial dilutions. The legend refers to % v/v, where 100% is the Turkevich synthesis product ([AuNP] ≈ 10 nM).

AuNP-Cit DLS

To determine the hydrodynamic diameter of AuNP-Cit particles, DLS measurements were performed.

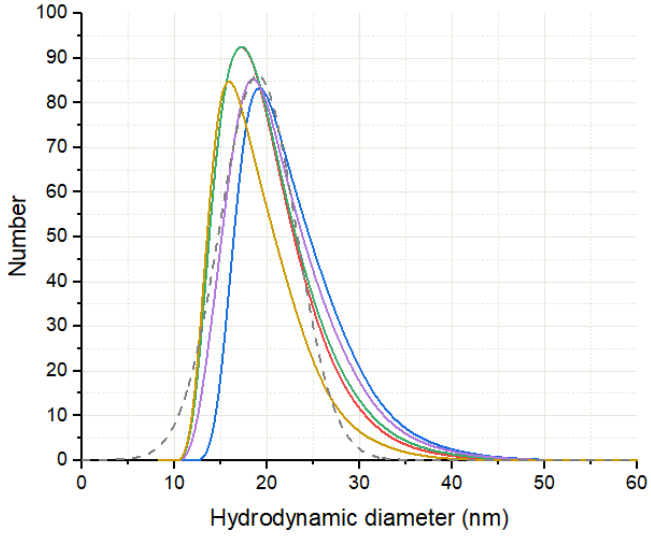

Figure SM-2. Number distribution as a function of hydrodynamic diameter of AuNP-Cit particles in suspension. Solid lines represent individual measurements () and the dashed line corresponds to the gaussian fitting of the average curve of all measurements (average curve not shown). Hydrodynamic diameter obtained: d_h = 19 ± 3 nm.

AuNP-Cit VS Ethanol proportion optimization

To determine the optimal AuNP-Cit VS Ethanol proportion, UV-Vis spectra were recorded at increasing proportion of EtOH, from (1:9) to (1:1) against AuNP.

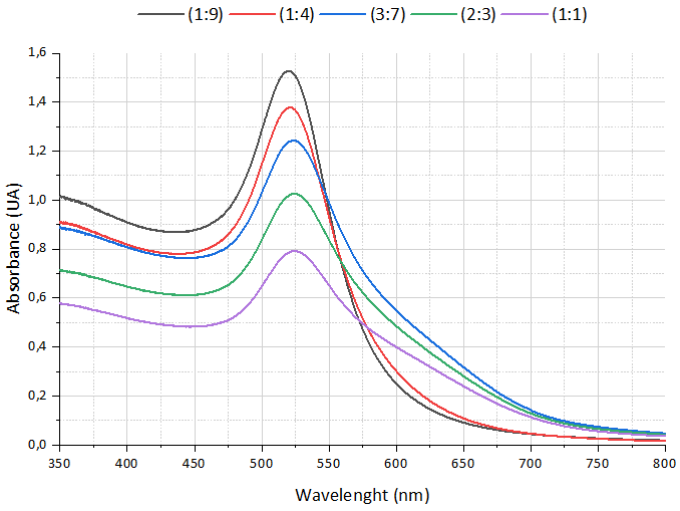

Figure SM-3. Visible spectra of AuNP-Cit with increasing proportion of EtOH (legend above graph).

AuNP-Cale UV-Vis and LSPR shift

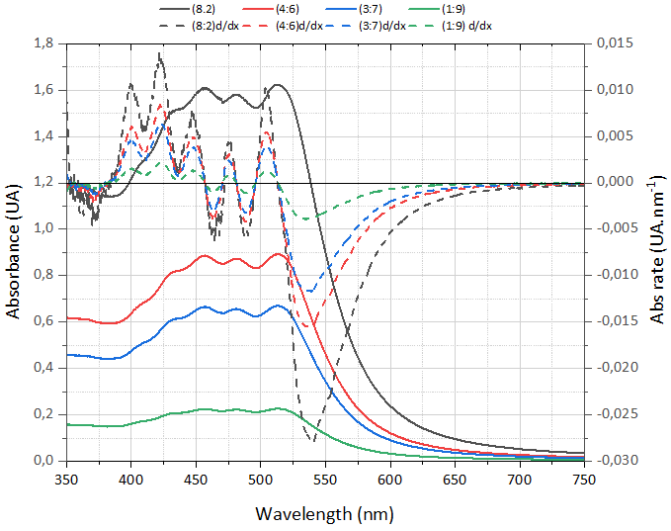

Figure SM-4. UV-Vis spectra of AuNP-Cale and it's first derivatives (denoted absorbance rates) with increasing dilution in water. Straight lines represent the UV-Vis spectra, while dashed lines represent the absorbance rates (legend above graph). An auxiliar axis at $d_{Abs}/d\lambda = 0$ was added to facilitate maxima's reading.